Effect of post-treatments and concentration of cotton linter cellulose nanocrystals on the properties of agar-based nanocomposite films

ARTICLE *in* CARBOHYDRATE POLYMERS · JULY 2015

Impact Factor: 4.07 · DOI: 10.1016/j.carbpol.2015.07.053

2 AUTHORS:

Ahmed A. Oun
Mokpo National University
3 PUBLICATIONS **8** CITATIONS
SEE PROFILE

Jong-Whan Rhim
Mokpo National University
137 PUBLICATIONS **3,255** CITATIONS
SEE PROFILE

Carbohydrate Polymers 134 (2015) 20–29

Contents lists available at ScienceDirect

Carbohydrate Polymers

journal homepage: www.elsevier.com/locate/carbpol

Effect of post-treatments and concentration of cotton linter cellulose nanocrystals on the properties of agar-based nanocomposite films

Ahmed A. Oun[a,b], Jong-Whan Rhim[a,*]

[a] Department of Food Engineering and Bionanocomposite Research Institute, Mokpo National University, 61 Dorimri, Chungkyemyon, Muangun, 534-729 Jeonnam, Republic of Korea
[b] Food Packaging and Engineering Department, Food Technology Research Institute, Agriculture Research Center, Giza, Egypt

ARTICLE INFO

Article history:
Received 2 April 2015
Received in revised form 10 June 2015
Accepted 15 July 2015
Available online 22 July 2015

Keywords:
Cotton linter
Cellulose nanocrystals
Effect of post-treatment
Agar
Sulfate groups
Nanocomposite films

ABSTRACT

Cellulose nanocrystals (CNCs) were prepared by acid hydrolysis of cotton linter pulp fibers and three different purification methods, i.e., without post purification (CNC1), dialyzed against distilled water (CNC2), and neutralized with NaOH (CNC3), and their effect on film properties was evaluated by preparation of agar/CNCs composite films. All the CNCs were rod in shape with diameter of 15–50 nm and length of 210–480 nm. FTIR result indicated that there was no distinctive differences in the chemical structure between CNCs and cotton linter cellulose fiber. No significant relationship was observed between the sulfate content and crystallinity index of CNCs. The CNC3 showed higher thermal stability than the other type of CNCs due to the less adverse effect on the thermal stability of sulfate groups induced by the neutralization with NaOH. The tensile strength (*TS*) of agar film increased by 15% with incorporation of 5 wt% of CNC3, on the contrary, it decreased by 10% and 15% with incorporation of CNC1 and CNC2, respectively. Other performance properties of agar/CNCs composite films such as optical and water vapor barrier properties showed that the CNC3 was more effective filler than the other CNCs. In the range of concentration of CNC3 tested (1–10 wt%), inclusion of 5 wt% of CNC3 was the maximum concentration for improving or maintaining film properties of the composite films. The neutralization of acid hydrolyzed cellulose using NaOH was simple and convenient for the preparation of CNC and bionanocomposite films.

1. Introduction

As the advent of nanotechnology, various types of nano-sized filler materials such as nanoclays, metallic nanoparticles, and nanocellulose have been exploited to improve properties of packaging materials such as physical, mechanical, and gas barrier properties (Rhim, Park, & Ha, 2013). Among the nanofiller materials, nanocellulose has attracted interest due to their unique features such as biodegradability, renewability, abundance with high modulus and mechanical strength, high specific surface area, and low density (Azizi Samir, Alloin, & Dufresne, 2005). Such properties made them attractive for their use in nanocomposite materials (Xu et al., 2013). Nanocellulose can be isolated from any cellulose-containing materials by various mechanical methods such as high-pressure homogenization, grinding, ultrasonication or high-speed blending (Li et al., 2012; Li et al., 2014), chemical methods including sulfuric acid, hydrochloric acid, or TEMPO (2,2,6,6-tetramethylpyperidine-L-oxyl) oxidation (Jiang & Hsieh, 2013; Rhim, Reddy, & Luo, 2015), enzyme-assisted hydrolysis (Henriksson, Henriksson, Berglund, & Lindstrorn, 2007), as well as a combination of two or several of the above mentioned methods (Alemdar & Sain, 2008; Chen et al., 2011). Nanocellulose materials obtained by the chemical methods are relatively uniform in size with high crystallinity (Jiang & Hsieh, 2013). Among the chemical methods, acid hydrolysis is the most widely used method to prepare cellulose nanocrystals (Jiang & Hsieh, 2013; Rhim et al., 2015). Strong acids such as hydrochloric acid and sulfuric acid can be used to prepare crystal forms of nanocelluose. Hydrolysis of cellulose fiber using hydrochloric acid produces nanocellulose with minimal surface charge, and the nanocrystals formed are inclined to aggregate due to lack of the electrostatic repulsion force between crystal particles (Wang, Ding, & Cheng, 2007). On the contrary, hydrolysis of cellulose fiber using sulfuric acid produces cellulose nanocrystals in a more stable colloidal suspension (Teixeira, Correa, Manzoli, Leite, Oliveira, & Mattoso, 2010) since the surface hydroxyl groups of cellulose fibers are esterified to form anionic sulfate ester groups (Beck-Candanedo, Roman, & Gray, 2005), however, the high sulfate content of the cellulose nanocrystals causes a decreased thermal

* Corresponding author. Fax: +82 61 454 1521.
E-mail addresses: jwrhim@mokpo.ac.kr, jwrhim@hanmail.net (J.-W. Rhim).

http://dx.doi.org/10.1016/j.carbpol.2015.07.053
0144-8617/

stability. Therefore, sulfuric acid hydrolysis have been widely used with various cellulose materials such as coconut husk fibers (Rosa et al., 2010), cotton linter (Morais et al., 2013), rice straw (Jiang & Hsieh, 2013), bacterial cellulose (Roman & Winter, 2004), wood (Beck-Candanedo et al., 2005), and agricultural processing waste (Rhim et al., 2015). However, the presently used acid hydrolysis method for the isolation of cellulose nanofiber has some limitations, such as prolonged time and cost to remove free sulfuric acid in the cellulose nanofiber after hydrolysis process, for their use in industrial scale. The free sulfuric acid in the cellulose nanofibers are usually removed by dialysis against water until they reach to neutral pH, which is costly and takes long time (more than two or three days). The presence of sulfate groups, the divalent group or anionic SO_4^{2-} or $-OSO_2O-$ of sulfuric acid and sulfates, on the surface of nanocellulose reduces interaction of the cellulose with other polymeric materials (Kontturi, Tammelin, & Osterberg, 2006). In addition, even low levels of sulfate groups onto the surface of fibers cause a significant decrease in the thermal stability of nanocellulose (Roman & Winter, 2004). To overcome such problem, cellulose nanocrystal suspension produced by mixed sulfuric acid and hydrochloric acid was adjusted to pH about 9 using sodium hydroxide, then washed with distilled water until to reach the neutrality (Wang et al., 2007). However, this process also took a long time. Compared with the time-consuming dialysis method, the chemical neutralization method is simple with less processing steps to prepare cellulose nanocrystals, especially this method is efficient when the cellulose nanofibers are used to make composite with other polymer and biopolymer materials. To the best of our knowledge, no work on the preparation of bionanocomposite blended with cellulose nanocrystals produced by this method has been reported.

In the present study, agar-based nanocomposite films were prepared by blending agar with cellulose nanocrystals isolated from cotton linter pulp using the acid hydrolysis and neutralization with NaOH. Agar has been chosen because it is not only renewable, biodegradable, biocompatible, and abundantly available, but also it has good film forming ability with high mechanical strength and moderate water resistance (Gimenez, Lopez de Lacey, Perez-Santín, Lopez-Caballero, & Montero, 2013). Agar has been used to form composite films with various biopolymers such as carrageenan and konjac glucomannan (Rhim & Wang, 2013), and gelatin (Gimenez et al., 2013) to improve physical and mechanical properties of the films. It has also been used as a carrier or matrix of antimicrobial materials such as grapefruit seed extract (Kanmani & Rhim, 2014), silver nanoparticles (Rhim, Wang, Lee, & Hong, 2014), copper nanoparticles (Shankar, Teng, & Rhim, 2014), and clay (Rhim, 2011). Cellulose nanocrystals have been used to improve mechanical and gas barrier properties of agar-based films (Reddy & Rhim, 2014). Cotton linters are short fibers adhered to cottonseed after ginning and obtained as leftover in the textile industry as they are too short for normal uses (Lu, Weng, & Cao, 2005; Savadekar, Karande, Vigneshwaran, Kadam, & Mhaske, 2014). Cotton linter contains high cellulose content (80% of holocellulose with 75% of α-cellulose) (Morais et al., 2013) compared with other natural resources. Cellulose nanocrystals isolated from cotton linter have been used as nanofiller to improve the properties of fish gelatin (Santos et al., 2014), chitosan (Li, Zhou, & Zhang, 2009), and thermoplastic starch (Savadekar et al., 2014) films.

Therefore the main objective of the present study was to test the efficiency of the proposed method of acid hydrolysis of cellulose fiber followed by neutralization with NaOH without tedious process of dialysis. Isolated cellulose nanocrystals were characterized by scanning electron microscopy (SEM), Fourier transform infrared spectroscopy (FT-IR), X-ray diffraction (XRD), and thermogravimetric analysis (TGA). The effect of sulfate content and concentration of nanocrystals on the mechanical properties, water vapor permeability (WVP), water contact angle (CA), surface color, transparency as well as SEM and XRD analysis of agar/cellulose nanocrystals composite films were also tested.

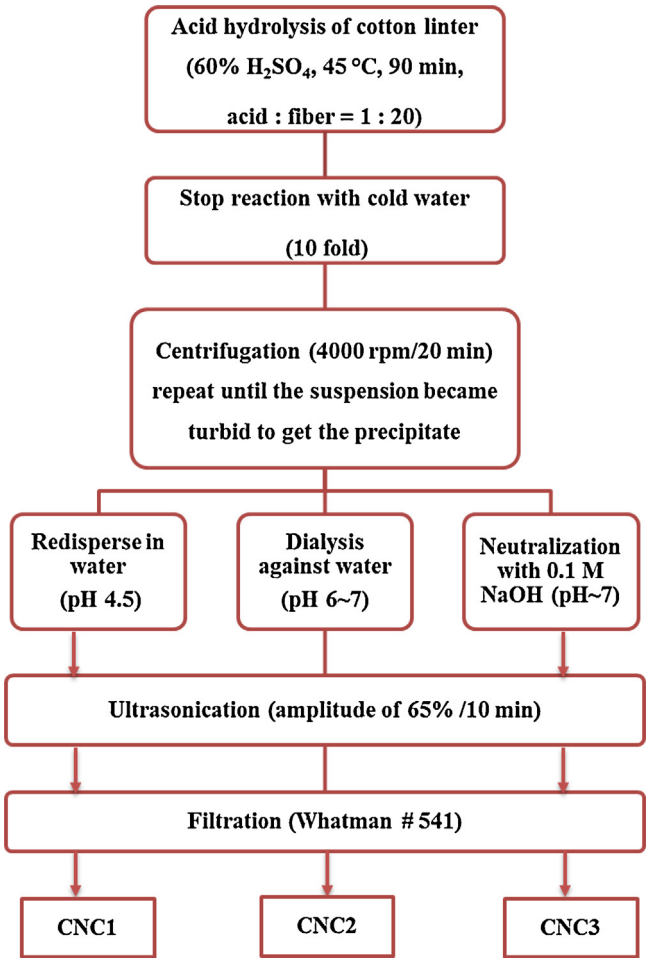

Fig. 1. Procedure for the preparation of cellulose nanocrystals (CNCs) from cotton linter pulp fiber.

2. Materials and methods

2.1. Materials

Food grade agar was obtained from Fine Agar Co., Ltd. (Damyang, Jeonnam, Korea). Glycerol was procured from Daejung Chemicals & Metals Co., Ltd. (Siheung, Gyeonggi-do, Korea). Sulfuric acid and sodium hydroxide were purchased from Duksan Pure Chemicals Co., Ltd (Ansan-city, Gyeonggi-do, South Korea). Cotton linter pulp (CLP-A; α-cellulose 99.1%, viscosity 8.4 cP, DPn 465, DPw 1745) was generously donated from COMSCO (Korea Minting and Security Printing Corporation, Daejeon, Korea).

2.2. Preparation of cellulose nanocrystals (CNCs)

Cotton linter pulp was ground to fine powder using a laboratory scale blender (Green Mix, model DA700-G, Artlon, Seoul, Korea), then cellulose nanocrystals (CNCs) were isolated from the fiber using acid hydrolysis and post-purification methods as shown in Fig. 1. The finely disintegrated cotton linter fiber was hydrolyzed with pre-heated 60% sulfuric acid with fiber to acid ratio of 1:20 at 45 °C for 90 min with strong agitation. The reaction was quenched by adding 10-fold of cold water and the suspension was centrifuged at 4000 rpm for 20 min using a bench–top centrifuge (Hanil

Scientific Centrifuge, Incheon, Gyeonggi-do, Korea), then washed with distilled water until the suspension became turbid with pH about 4. The next step of purification of CNC was performed using three different post-purification methods for the preparation of CNCs. First, the precipitate was suspended in distilled water and was designated as CNC1 without further purification step (pH about 4.5). Second, the precipitate was suspended in distilled water and dialyzed against water using a dialysis tubing (cellulose membrane with molecular cut-off of 14,000, Sigma–Aldrich, St. Louis, MO, USA) until neutrality was attained for 2–3 days (pH 6–7), which was designated as CNC2. Third, the precipitate was suspended in distilled water and neutralized with 0.1 M of NaOH solution, which was designated as CNC3 (pH 7). To obtain well dispersed CNC colloidal suspensions, all the CNC suspensions were sonicated using a high intensity ultrasonic processor (Model VCX 750, Sonics & Materials Inc., New Town, CT, USA) for 10 min (pulse 5 s on/2 s off) with an amplitude of 65% in an ice water bath. After that, the suspensions were filtered using a filter paper (Whatman #541) to remove agglomerated and large particles, and stored in a refrigerator at 4 °C before further characterization or use for the preparation of composite films.

2.3. Preparation of films

Agar and agar/CNCs composite films were prepared by solvent casting method (Reddy & Rhim, 2014). The control agar film solution was prepared by dissolving 4 g of agar in 150 mL of distilled water with 1.6 g of glycerol as plasticizer for 30 min at 95 °C using a magnetic stirrer until to get clear solution. In addition, two series of agar/CNC composite films were prepared. To test the effect of the type of CNCs, agar/CNCs composite films including 5 wt% of each type of CNCs were prepared, and to test the effect of the concentration of CNC, agar/CNC composite films including various concentration of CNC3 (1, 3, 5, and 10 wt% based on agar weight) were prepared. For the preparation of agar/CNC composite film solutions, determined amount of CNC was dissolved into 150 mL of distilled water for 2 h with stirring using a magnetic stirrer. Then, the suspension was homogenized at 10,000 rpm for 10 min using a high shear mixer (T25 basic, Ika Labotechnik, Janke & Kunkel Gmbh & Co., KG Staufen, Germany). After that, 4 g of agar and 1.6 g of glycerol were added to the CNC suspensions and heated at 95 °C for 30 min to get the film solution. All the film solutions were cast onto a balance leveled Teflon film (Cole-Parmer Instrument Co., Chicago, IL, USA) coated glass plate and dried at room temperature (22 ± 3 °C). The dried films were peeled off from the casting plate and conditioned in a humidity chamber controlled at 25 °C and 50 % relative humidity (RH) for at least 3 days before further analysis.

2.4. Characterization of cellulose fibers

The microstructure of cotton linter fiber and its CNCs, and agar/CNCs composites films were observed using a scanning electron microscopy (FE-SEM, S-4800, Hitachi Co., Ltd., Matsuda, Japan) operated at an acceleration voltage of 10 kV and current of 10 μA after coating the samples with osmium (Os) using a vacuum sputter coater. For the determination of dimensions of the CNC, the CNC was dispersed in distilled water to make 0.01 wt% of CNC solution and about 10 μL of the CNC solution was deposited onto a 300 mesh nickel grid. After 20 min, the excess liquid was removed by blotting with a filter paper and allowed to dry and observed the microstructure with a scanning transmission electron microscopy (STEM) using the FE-SEM instrument in the transmission mode. The length and diameter of CNCs were determined using the internal scale of the instrument.

The elemental composition of the CNCs was analyzed by an energy dispersive X-ray spectroscopy (EDX) in the SEM instrument (FE-SEM, S-4800, Hitachi Co., Ltd., Matsuda, Japan).

Fourier transform infrared spectroscopy (FTIR) was conducted using an attenuated total reflectance-Fourier transform infrared (ATR-FTIR) spectrophotometer (TENSOR 37 spectrophotometer with OPUS 6.0 software, Billerica, MA, USA). Dried CNCs samples were ground and pelletized using KBr (1:100 w/w) and their spectra were recorded in the range of 4000–600 cm^{-1}.

X-ray diffraction (XRD) patterns of the cotton linter pulp fiber, CNCs, and agar/CNCs composite films were analyzed using a XRD diffractometer (PANalytical Xpert Pro MRD diffractometer, Amsterdam, Netherlands), operated at 40 kV and 30 mA, equipped with Cu Kα radiation at a wavelength of 1.54056 Å and a nickel monochromator filtering wave. The samples were scanned over the range of $2\theta = 10–50°$ with scanning rate of 0.4°/min at room temperature. The crystallinity index (CI) was calculated using following equation (Gumuskaya, Usta, & Kirci, 2003):

$$CI = \frac{I_{200} - I_{am}}{I_{200}} \quad (1)$$

where I_{200} is the maximum intensity of the diffraction peak (200 peak) at $2\theta = 22.7°$ and I_{am} is the minimum intensity corresponds to the amorphous structure which was located at $2\theta = 19°$. The crystallite size (D) of the CNC was calculated by the Debye–Scherrer equation (Nazir, Wahjoedi, Yussof, & Abdullah, 2013).

$$D = \frac{K\lambda}{\beta_{1/2} \ \mathrm{Cos}\ \theta} \quad (2)$$

where K is the Scherrer constant (0.94), λ is the X-ray wavelength (λ = 1.54056 Å), $\beta_{1/2}$ is the full width at the half maximum (FWHM) of the XRD peak, and θ is the Bragg's angle.

Thermal stability of cotton linter fiber and its CNCs was analyzed using a thermogravimetric analyzer (Hi-Res TGA 2950, TA Instrument, New Castle, DE, USA). About 5 mg of samples were taken in a standard aluminum cup and an empty cup was used as a reference, and heated from room temperature to 600 °C at rate of 10 °C/min under a nitrogen flow of 50 cm^3/min. Derivative form of TGA (DTG) was obtained using differentials of TGA values, calculated using a central finite difference method as follows:

$$\mathrm{DTG} = (w_{t+\Delta t} - w_{t-\Delta t})/2\Delta t \quad (3)$$

where $w_{t+\Delta t}$ and $w_{t-\Delta t}$ are the residual weight of sample at time $t + \Delta t$ and $t - \Delta t$, respectively, and Δt is the time interval for reading residual sample weight (Rhim et al., 2015). The maximum decomposition temperature (T_{max}) of cotton linter fiber and CNCs was obtained from DTG curve and the char content and the weight loss (%) were determined from the TGA curve.

2.5. Color and transparency

Surface color of the agar and agar/CNCs composite films was evaluated using a Chroma meter (Minolta, CR-200, Tokyo, Japan). A white color plate ($L = 97.75$, $a = -0.49$, and $b = 1.96$) was used as a standard background color. Color parameters such as L (lightness), a (greenness–redness), and b (blueness–yellowness) values were determined by average of five readings from each film sample. The total color difference (ΔE) of the film was calculated as follows:

$$\Delta E = \sqrt{(\Delta L)^2 + (\Delta a)^2} + (\Delta b)^2 \quad (4)$$

where ΔL, Δa, and Δb are the difference between each color values of standard color plate and film sample, respectively. Transparency of the film samples was determined by measuring percent transmittance at 660 nm (T_{660}) and 280 nm (T_{280}) using a UV/vis

spectrophotometer (Model 8451A, Hewlett-Packard Co., Santa Alara, CA, USA) (Rhim et al., 2015).

2.6. Mechanical properties

Thickness of the film samples was measured using a hand-held micrometer (Digimatic micrometer, Quantumike IP65, Mitutoyo, Japan) at an accuracy of 0.001 mm. The average values of five random measurements were taken for each film sample. Each film was cut into rectangular strips (2.54 cm × 15 cm) using a precision double blade cutter (ModelLB.02/A, Metrotech, S.A., San Sebastian, Spain), and the tensile strength (TS), elongation at break (E), and elastic modulus (EM) of each film was measured according to the standard test method of ASTM D 882-88 using an Instron Universal Testing Machine (Model 5565, Instron Engineering Corporation, Canton, MA, USA). The machine was operated in tensile mode with an initial grip separation of 50 mm and crosshead speed of 50 mm/min. The TS was determined by dividing the maximum load (N) by the initial cross-sectional area (m^2) of the films and expressed in MPa. The E (%) was determined by dividing the extension at the rupture of the film by the initial length of the film (50 mm) multiplied by 100. The EM (MPa) was determined from the slope of the linear portion of the stress–strain curve, which corresponds to the stress divided by the strain of the film sample. Ten measurements were carried out for each film and the average values were presented.

2.7. Water vapor permeability (WVP)

The water vapor permeability (WVP) of the films was determined gravimetrically according to the standard method of ASTM E96-95 with slight modification (Gennadios, Weller, & Gooding, 1994). The films were cut into square pieces (7 cm × 7 cm) and mounted directly on the top of WVP cups (2.5 cm in depth and 6.8 cm of diameter) containing 18 mL of distilled water. The level of water was up to 1 cm underneath the film and each cup with the film was tightened with screw to prevent leakage of water vapor. The cups were placed in a constant temperature and humidity chamber (model FX 1077, Jeio Tech Co. Ltd., Ansan, Korea) controlled at 25 °C and 50% RH with air movement of 198 m/min. The weight of the cups was measured every hour for a period of 8 h and weight loss from each cup was measured. Water vapor transmission rate (WVTR) was calculated from the slopes (linear) of the steady state portion of weight loss of the cup versus time curve. Then, the WVP of the films was calculated in g.m/m^2.Pa.s as follows:

$$\mathrm{WVP} = \mathrm{WVTR} \times L)/\Delta p (5)$$

where WVTR was the measured water vapor transmission rate (g/m^2.s) through a film, L was mean thickness of the film (m) and Δp was the partial water vapor pressure difference (Pa) across the two sides of the film.

2.8. Water contact angle

Water contact angle (CA), a measure of hydrophilicity/hydrophobicity of film samples, of agar and agar/CNCs composite films was measured using a water contact angle analyzer (model Phoenix 150, Surface Electro Optics Co., Ltd., Kunpo, Gyeonggi-do, Korea). The film samples were cut into rectangular piece (3 cm × 10 cm) and placed on the horizontal movable stage made of black Teflon coated steel. A drop of water (about 10 μL) was placed on the surface of the film using a microsyringe and contact angle was measured on both sides of the water drop to assume symmetry and horizontal level. The average values of three measurements of each sample were presented as the degree of CA.

2.9. Statistical analysis

Measurements of film properties were performed in triplicate with individually prepared film samples and data were expressed as the mean ± SD (standard deviation). One-way analysis of variance (ANOVA) was conducted and significant difference ($p < 0.05$) between each mean property value was determined with the Duncan's multiple range tests using a statistical software package (SPSS Inc., Chicago, IL, USA).

3. Results and discussion

3.1. Morphology and element analysis

Microstructure of cotton linter pulp fiber and its CNCs observed by SEM with their appearance were shown in Fig. 2. The native cotton linter fibers were long fibrous forms with rough surface and their diameter was in the range of 14–30 μm. Diameter and length of cellulosic materials before acid hydrolysis depend on the pretreatments, the types of grinding machine and the size of sieves used, so the resulting dimensions of crystalline cellulose nanocrystals after acid hydrolysis are also influenced by such treatments. Similar size of cotton fibers has been reported, i.e., Morais et al., (2013) obtained cotton fibers with average diameter of 23.04 μm, and

Teixeira et al., (2010) obtained cotton fibers with diameter of 13–22 μm from different white and naturally colored cotton fibers. The CNCs obtained after acid hydrolysis showed well-dispersed suspension with white colloidal gel appearance as shown in the subset picture of Fig. 2. It was mainly due to that the electrostatic repulsion, induced by the sulfate groups grafted onto the surface of cellulose nanocrystals, prevented the suspension from aggregation or sedimentation (; Lu et al., 2005). The crystalline cellulose nanocrystals (CNCs) were rod-like in shape with diameter of 15–50 nm and length of 210–480 nm (aspect ratio about 9). Though several studies have been performed for isolation of cellulose nanocrystals from cotton linter, their length and diameter of CNC were varied depending on the source of fiber and isolation methods (Chang, Wang, Hung, & Perng, 2010).

Interestingly, the amount of sulfate groups in the CNCs was varied depending on the post-purification of CNCs. The existence and content of sulfate groups in the CNCs were evaluated using EDS and the results are shown in Fig. 2. CNC1 obtained without any further treatment after acid hydrolysis showed the sulfur with the content of 0.19% which was due to presence of residual sulfate groups in the nanocrystals suspension. On the contrary, CNC2 obtained by dialysis of acid hydrolyzed CNC against distilled water showed decreased sulfur content of 0.05%. No sulfur peak was observed in the CNC3 obtained by neutralization with NaOH, which was mainly due to the conversion of sulfate ester groups to monosodium cellulose sulfate esters (Chang et al., 2010). Sulfur content was influenced by the post-purification method as well as other factors such as source of cellulose, source of cellulose, and hydrolysis time (Lu & Hsieh 2012).

3.2. Fourier transform infrared (FTIR) analysis

FTIR analysis was performed to analyze any probable change in the chemical structure between cotton linter fiber and its nanocrystals, and the results are shown in Fig. 3. The broad bands in the region of 3650–3000 cm^{-1} are related to O—H stretching vibrations and absorption peak at 2900 cm^{-1} correspond to C-H stretching vibrations of cellulose in the fiber and CNCs

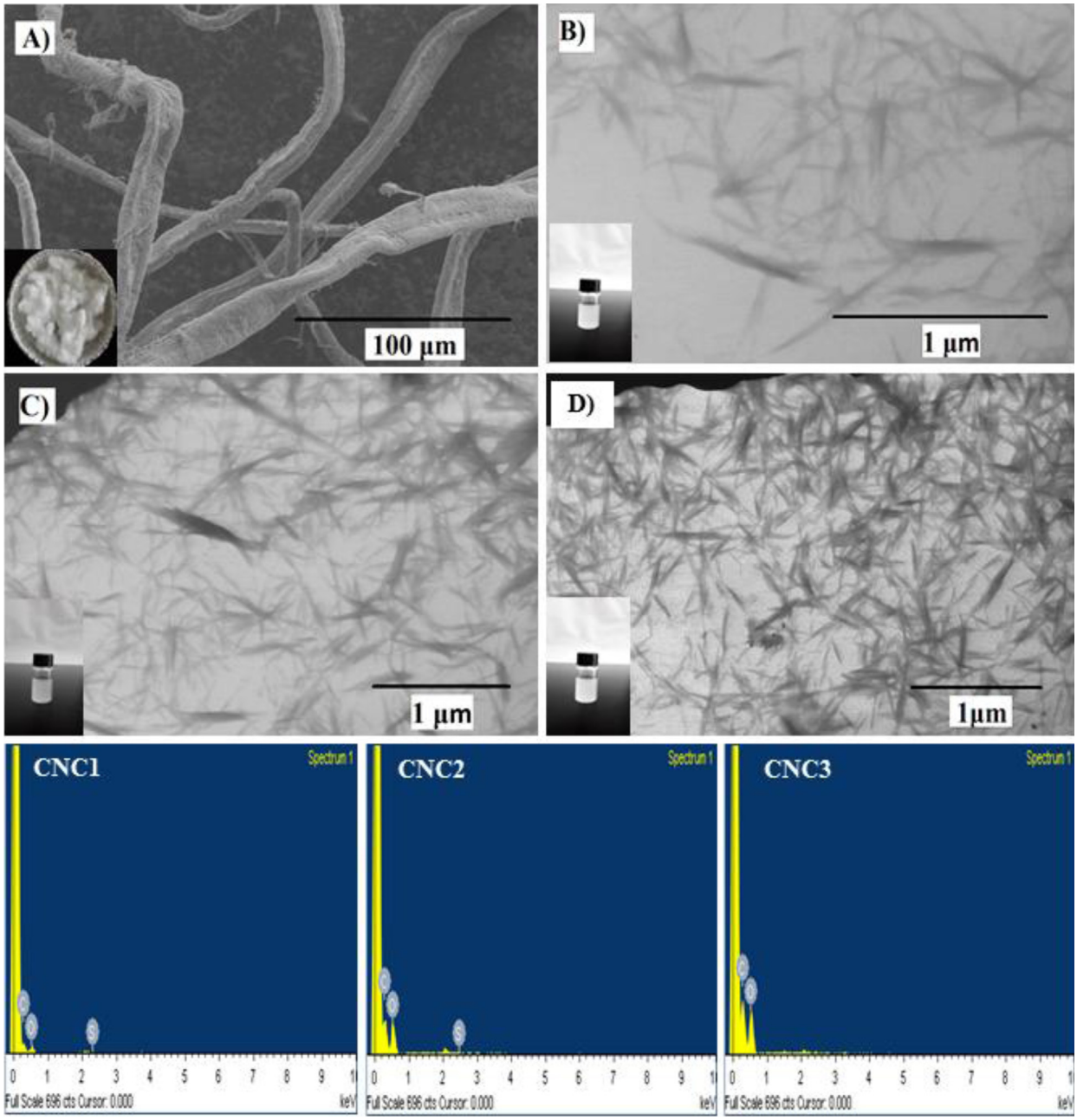

Fig. 2. SEM images of (A) cotton linter fiber and STEM of (B) CNC1 (C) CNC2 and (D) CNC3, and energy dispersive X-ray spectroscopy (EDX) of CNC1–CNC3.

(Li et al., 2009; Lu & Hsieh 2010; Reddy, Maheswari, Reddy, Guduri, & Rajulu, 2010). The peak at 1641 cm^{-1} is related to adsorbed water in the cellulose (Lu & Hsieh 2010). The peak at 896 cm^{-1} indicates the purity of the cellulose which resulted from C—H vibration found in the fibers and CNC (Alemdar & Sain, 2008). Usually, the native cellulose is composed of two crystalline forms (one-chain triclinic structure, Iα) and (two-chain monoclinic structure, Iβ), which depend on the origin of cellulose. The Iβ crystalline form is known to prevail in the cotton cellulose (Azizi Samir et al., 2005). The peak at 710 cm^{-1} is related to crystalline Iβ form which was found in the cotton linter fiber and its CNCs (Wada, Kondo, & Okano, 2003). The FT-IR spectra of the CNCs were not changed significantly compared to that of the cotton linter fiber except peak intensities, which indicates that there was no structural changes after acid hydrolysis of the fiber.

3.3. X-ray diffraction analysis

XRD was used to investigate crystalline structure of cotton linter fiber, CNCs and agar/CNCs nanocomposite films, and the results are shown in Fig. 4. Both cotton linter fiber and CNCs exhibited a well-defined main peak at $2\theta = 22.7^{\circ}$ and two broad peaks around 14° and 17°, which is a characteristic diffraction pattern of cellulose I (Wada, Heux, & Sugiyama, 2004; Wang et al., 2007). All CNCs obtained by acid hydrolysis showed narrow and sharp peaks with higher peak intensity than those of non-hydrolyzed counterpart, which indicates increased crystallinity of the CNCs. The crystallinity index (CI) of cotton linter fiber and CNCs was calculated using Eq. (1), and found that the CI of cotton linter fiber was 0.73 and it increased after acid hydrolysis up to 0.87–0.89 for CNC1–CNC3, respectively. The increase in the crystallinity of CNC has been resulted from the removal of amorphous regions from the native cotton linter fiber

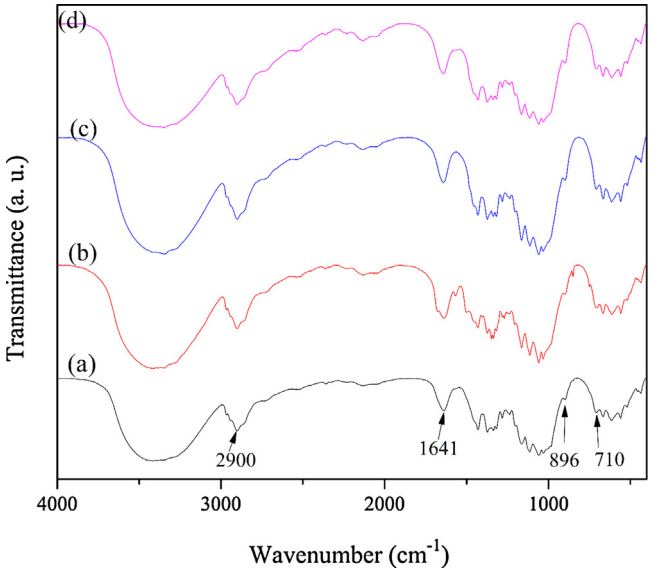

Fig. 3. FTIR spectra of (a) cotton linter fiber, (b) CNC1, (c) CNC2, and (d) CNC3.

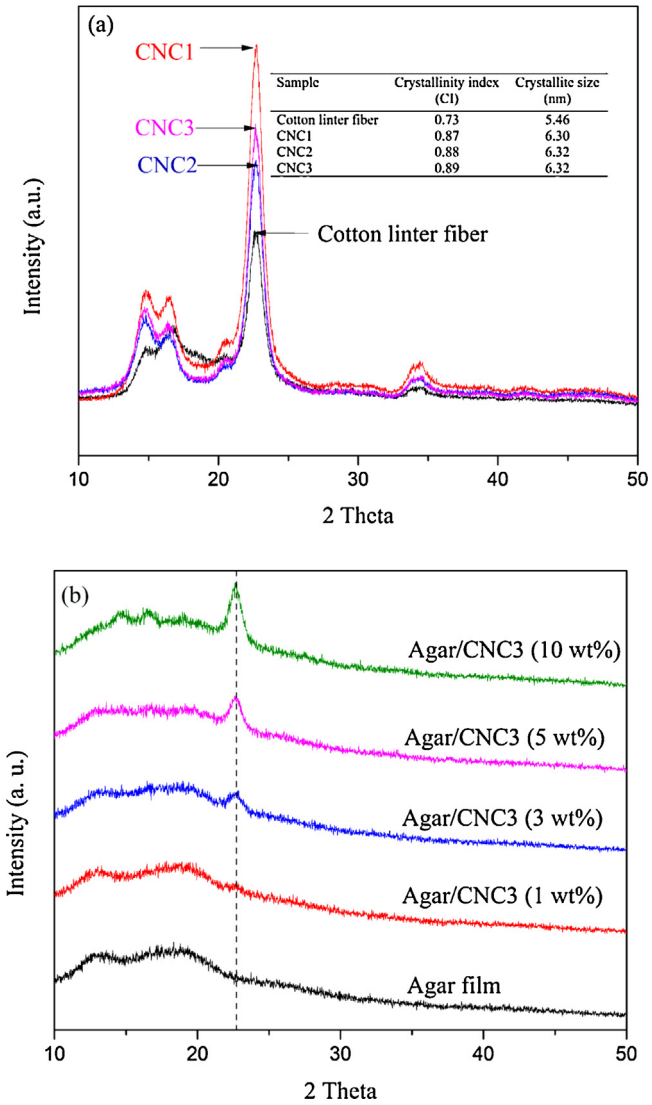

Sample	Crystallinity index (CI)	Crystallite size (nm)
Cotton linter fiber	0.73	5.46
CNC1	0.87	6.30
CNC2	0.88	6.32
CNC3	0.89	6.32

Fig. 4. XRD patterns of (a) cotton linter fiber and CNCs, and (b) Agar/CNC3 nanocomposite films.

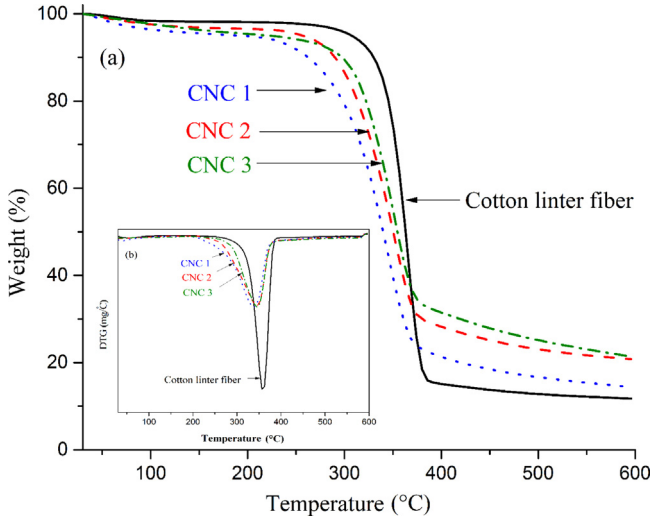

Fig. 5. TGA thermograms and DTGA curves of cotton linter fiber and its cellulose nanocrystals.

through acid hydrolysis (Lu & Hsieh 2010). The difference in crystallinity was not significant, even though there was difference in sulfur content among three CNCs as observed in the EDX results. This result suggests that the sulfur content may not influence on the crystallinity of the acid hydrolyzed CNCs. Teixeira et al. (2010) also reported that the CI of both white and brown cotton linter nanofibers was 0.91, even though their sulfur content was different, i.e., 2.18% and 1.50% for white and brown cotton linter nanofibers, respectively. The crystallite size of cotton linter fiber and the CNCs was determined using the Debye–Scherrer equation [Eq. (2)]. The crystallite size of cotton linter fiber was 5.46 nm and it increased up to 6.30, 6.32, and 6.32 nm for CNC1, CNC2, and CNC3, respectively, after aid hydrolysis. Similar results of increase in crystal size of CNC obtained by acid hydrolysis have been frequently observed with other cellulosic materials (Maiti et al., 2013; Reddy & Rhim, 2014).

3.4. Thermal stability

Thermal stability of cotton linter fiber and its CNCs was evaluated using TGA analysis and the results are shown in Fig. 5. The TGA thermograms and DTG curves exhibited clearly the weight decreasing patterns and the maximum temperature (T_{max}) for the thermal decomposition of the fibers, respectively. Generally, cotton linter fiber and CNCs showed two steps of weight loss during thermal degradation. The first step of decrease in weight was observed at temperature around 80–120 °C with the weight loss of 1.6, 3.6, 2.4, and 2.3% for the cotton linter fiber, CNC1–CNC3, respectively. The weight loss in this step was mainly attributed to the evaporation of water absorbed in the fibers. The CNC1 exhibited the highest weight loss, which might be due to the presence of polar sulfate groups on the surface of nanocrystals as shown in the results of EDS analysis. A major weight decrease was observed in the second step of weight loss around 220–400 °C. The weight loss in this step was mainly due to the thermal degradation of cellulosic materials (Roman & Winter, 2004; Wang et al., 2007).

In this step, the thermal degradation pattern of CNCs was clearly different from that of cotton linter fiber, i.e., the onset temperature (T_{onset}) of thermal destruction of the CNCs (228, 258, and 275 °C for CNC1, CNC2, and CNC3, respectively) decreased compared to than that of the cotton linter fiber (293 °C) and their maximum degradation temperature (T_{max}; 339, 345, and 345 °C for CNC1, CNC2, and CNC3, respectively) was lower than that of the cotton linter fiber

(357 °C). Such decrease in thermal stability of the CNCs is presumably due to the gaining sulfate groups on the surface of the CNCs as well as removal of thermostable minerals during acid hydrolysis of the cotton linter fiber (Morais et al., 2013; Roman & Winter, 2004). In addition, the increased surface area of the CNCs might absorb more heat energy to induce their thermal destruction (Lu & Hsieh 2010). The effect of sulfate groups on the thermal stability was clearly observed between the three CNCs. The T_{onset} of CNC1 (228 °C) was the lowest due to their higher sulfur content compared to CNC2 and CNC3. On the contrary, T_{onset} of CNC3 increased profoundly up to 275 °C. The replacement of alkaline ion (Na^+) with the hydrogen ion (H^+) inhibited the dehydration catalyzed by the sulfuric acid (Rosa et al., 2010; Wang et al., 2007). The final residue left at 600 °C was 11.7, 14.4, 20.8 and 21.4% for cotton linter fiber, CNC1, CNC2 and CNC3, respectively. The final residue was higher in the CNCs than in the cotton linter samples, which was attributed to that the sulfate groups in the CNCs acted as a flame retardant (Roman & Winter, 2004). The differences in final residue left at 600 °C among the CNCs might be related to the variance in the size of CNCs since nanocellulose with small size is known to facilitate the char residue formation (Wang et al., 2007). Similar thermal degradation behavior has been observed previously with cotton linter crystalline cellulose isolated by sulfuric acid hydrolysis (Lu & Hsieh 2010; Teixeira et al., 2010).

3.5. Apparent color and transparency of films

The surface color and transparency of the agar and agar/CNC composite were determined by Hunter Lab-values and percent transmittance at 280 nm and 660 nm, respectively. Surface color and transparency of agar films were significantly affected by the addition of CNC as shown in Table 1.

The control agar film was flexible and transparent with high transmittance against both UV- and visible light (56.5 and 88.3% of T_{280} and T_{660}, respectively), however, Hunter *L*-(lightness) and *a*-values (green/redness) decreased and *b*-values (blue/yellowness) increased and consequently the total color difference (ΔE) increased significantly ($p < 0.05$) after blending with 5 wt% of all types of CNCs. More significant change was observed in the light transmittance, i.e., both transmittance of films (T_{280} and T_{660}) decreased from 56.5% and 88.3% down to 31.2%–38.8% and 58.7%–72.1% depending on the type of CNCs, respectively. This is mainly due to that the rigid cellulose nanocrystals hinder the light passage (Savadekar et al., 2014). Similar results have been frequently observed that the cellulose nanocrystals dispersed into biopolymer films lead to decrease in their transparency (Li et al., 2009; Shankar, Reddy, Rhim, & Kim, 2015). It is interesting to note that the transparency of the agar/CNC3 composite film decreased least among the CNCs tested. Such film with prevention of UV transmission without sacrificing transparency is desirable for the use as see-through and UV-screening packaging applications.

The effect of CNC3 concentration was tested with agar/CNC3 composite films prepared with various concentration of CNCs, and the results also shown in Table 1. Apparent color properties such as Hunter *L*, *a*, *b*- and ΔE values changed depending on the CNC3 concentration. Transmittance to both UV- and visible light of the composite films decreased linearly with increase in CNC concentration. The linear relationship could be expressed as follows:

$$T_{280}(\%) = -2.65x + 54.76 (R^2 = 0.97)$$

$$T_{660}(\%) = -3.09x + 87.98 (R^2 = 1.00)$$

where *x* is wt% of CNCs. Such linear relationship of transmittance and CNC has been also observed agar and mulberry pulp nanocellulose composite films (Reddy & Rhim, 2014). The decrease in the transmittance of the CNC incorporated films was mainly due to the rigid cellulose nanocrystals which hindered the light passage through the film (Savadekar et al., 2014). This is more intensified at higher concentration of CNCs due to agglomeration and entanglement of CNCs (Xu et al., 2013).

3.6. X-ray diffraction pattern and morphology of films

The X-ray diffraction patterns of agar and agar/CNC3 composite films are also shown in Fig. 4(b). Agar/CNC3 composite films exhibited characteristic peak at $2\theta = 22.7^\circ$ and the peak intensity increased with increase in the content of CNC, however, the agar control film did not show any diffraction peak at $2\theta = 22.7^\circ$ as expected. This XRD results also indicates that the CNCs are well distributed throughout the polymer matrix.

The distribution of CNC in the polymer matrix and their interaction were investigated by observing microstructure of both surface and cross-section of composite films using SEM analysis and the results are shown in Fig. 6. SEM images of surface and cross-section indicated that the control agar film was homogeneous and smooth in surface. Though the surface of Agar/CNC composite films became rougher than that of the control agar film, the CNC particles have been well dispersed in the polymer matrix. This indicates the CNCs were compatible with the polymer matrix at the level of 5 wt%. The composite film prepared with CNC3 was more smooth and homogeneous than other types of CNCs, which indicates that the CNC3 has high dispersibility and compatibility with the polymer matrix. However, when the CNC concentration increased to 10 wt%, the surface of composite film became less homogeneous and discontinuous voids were appeared between CNCs and the polymer matrix as shown in the cross-sectional view of SEM image [Fig. 6(e)]. This was mainly due to the agglomeration of CNCs in the polymer matrix at high concentration (Savadekar et al., 2014) as well as high salt content in CNC3 at 10 wt%. Generally at high concentration, cellulose nanocrystals tend to agglomerate due to their high hydroxyl content (Bledzki & Gassan, 1999) upon drying. Agglomeration of nanocellulose in a biopolymer matrix has been observed at high concentration of nanocellulose more than 5 wt% in the preparation of agar/mulberry pulp nanocellulose composite films (Reddy & Rhim, 2014).

3.7. Mechanical properties of films

Mechanical properties of agar and agar/CNCs composite films are presented in Table 2.

The thickness of agar film increased significantly ($p < 0.05$) after blending with 5 wt% of CNCs, which was mainly due to the increase in the solid content of the film (Reddy & Rhim, 2014). Difference in film thickness among the composite films with the same concentration (5 wt%) of CNCs might be attributed to the different surface roughness as observed in the SEM images (Chinga-Carrasco & Syverud, 2010). When only the CNC3 was used with varying concentration, the film thickness increased with increase in the CNC content. The tensile properties such as strength, flexibility, and stiffness of agar/CNCs composite films determined by the TS, E, and EM, respectively, were dependent on the type of CNCs. The strength and stiffness of the composite films blended with 5 wt% of CNC1 and CNC2 decreased significantly ($p < 0.05$), however, those of agar/CNC3 composite film increased significantly compared to those of the control agar film. The decrease in TS of composite films blended with CNC1 and CNC2 might be attributed to lower intermolecular interactions between the cellulose nanocrystals and agar matrix than CNC3 (Rhim et al., 2015). Presence of sulfate groups on the surface of CNC1 and CNC2 might reduce interaction of the CNC with polymer matrix (Kontturi et al., 2006). The increased tensile strength of agar/CNC3 composite film may be

Table 1
Apparent color and transparency of agar and agar/CNCs composite films.[a]

Film	L	a	b	ΔE	T_{280} (%)	T_{660} (%)
Agar	92.68 ± 0.15[a]	−0.55 ± 0.03[a]	4.80 ± 0.34[d]	2.68 ± 0.34[c]	56.5 ± 0.2[a]	88.3 ± 0.1a
Agar/CNC1(5%)	92.09 ± 0.14[c]	-0.69 ± 0.01[b]	5.66 ± 0.17[b]	3.97 ± 0.21[a]	32.0 ± 0.4[c,d]	58.9 ± 0.2[c]
Agar/CNC2(5%)	92.05 ± 0.12[c]	−0.67 ± 0.01[b]	5.84 ± 0.14[a]	3.88 ± 0.19[a]	31.2 ± 0.6[d]	58.7 ± 0.3[c]
Agar/CNC3(5%)	92.41 ± 0.22[b]	−0.72 ± 0.02[c]	5.52 ± 0.15[c]	3.38 ± 0.26[b]	38.7 ± 1.7[b]	72.1 ± 1.2[b]
Agar/CNC3(1%)	92.60 ± 0.25[a]	−0.61 ± 0.02[b]	5.01 ± 0.26[d]	2.88 ± 0.32[c]	52.0 ± 0.4[b]	84.2 ± 0.1[b]
Agar/CNC3(3%)	92.42 ± 0.17[b]	−0.66 ± 0.03[c]	5.20 ± 0.33[c]	3.14 ± 0.36[b]	46.5 ± 0.2[c]	79.4 ± 0.4[c]
Agar/CNC3(5%)	92.41 ± 0.22[b]	−0.72 ± 0.02[d]	5.52 ± 0.15[b]	3.38 ± 0.26[b]	38.7 ± 1.7[d]	72.1 ± 1.2[d]
Agar/CNC3(10%)	91.70 ± 0.08[c]	-0.78 ± 0.01[e]	6.62 ± 0.12[a]	4.16 ± 0.13[a]	29.8 ± 1.2[e]	57.1 ± 1.7[e]

[a] Each value is the mean of three replicates with the standard deviation. Any two means in the same column followed by the same letter are not significantly ($p > 0.05$) different by Duncan's multiple range test. L: lightness, a: greenness–redness, b: blueness–yellowness, ΔE: total color difference, T_{280} and T_{660}: transmittance at 280 nm and 660 nm, respectively.

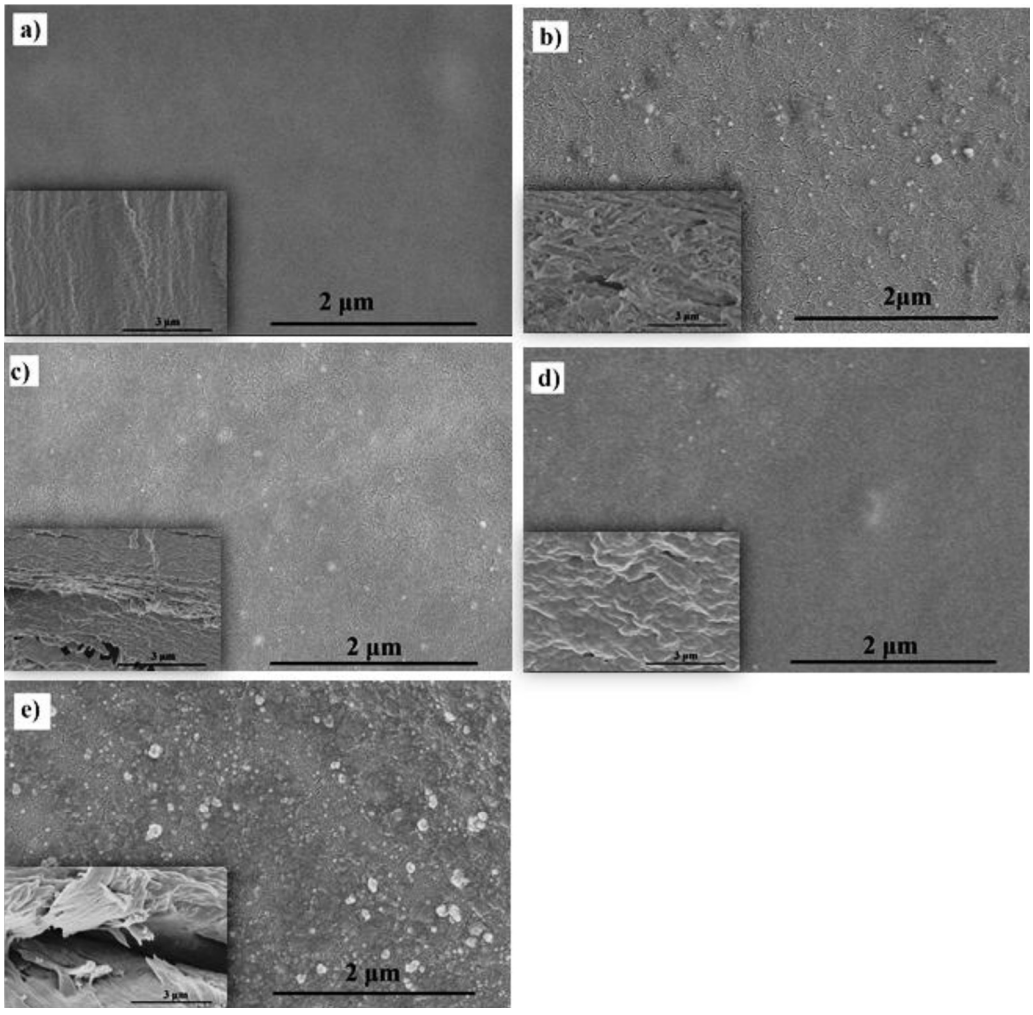

Fig. 6. SEM images of the surface and cross section of (a) agar film, (b) agar/CNC1(5 wt%), (c) agar/CNC2(5 wt%), (d) agar/CNC3(5 wt%), and (e) agar/CNC3(10 wt%).

Table 2
Mechanical properties of agar and agar/CNCs composite films.[a]

Film	Thickness (µm)	TS (MPa)	E (%)	EM (GPa)
Agar	50.9 ± 1.2[d]	29.3 ± 1.53[b]	29.4 ± 1.8[b]	0.63 ± 0.07[b]
Agar/CNC1(5%)	66.3 ± 1.9[a]	26.3 ± 0.3[c]	29.4 ± 1.2[b]	0.55 ± 0.01[c]
Agar/CNC2(5%)	56.8 ± 0.6[b]	24.9 ± 0.6[c]	29.6 ± 1.2[b]	0.56 ± 0.03[c]
Agar/CNC3(5%)	52.2 ± 0.1[c]	33.7 ± 1.5[a]	30.7 ± 0.4[a]	0.71 ± 0.01[a]
Agar/CNC3(1%)	51.4 ± 0.2[c]	32.7 ± 2.3[b,a]	31.2 ± 1.2[a]	0.71 ± 0.01[b]
Agar/CNC3(3%)	52.0 ± 1.2[b]	33.0 ± 1.2[b,a]	30.9 ± 1.6[a,b]	0.69 ± 0.20[b]
Agar/CNC3(5%)	52.2 ± 0.1[b]	33.7 ± 1.5[a]	30.7 ± 0.4[b,c]	0.72 ± 0.01[a]
Agar/CNC3(10%)	67.8 ± 1.7[a]	22.7 ± 0.5[c]	20.1 ± 1.5[d]	0.61 ± 0.01[d]

[a] Each value is the mean of three replicates with the standard deviation. Any two means in the same column followed by the same letter are not significantly ($p > 0.05$) different by Duncan's multiple range test.

Table 3
Water vapor permeability (WVP) and water contact angle (CA) of agar and agar/CNCs composite films.[a]

Film	WVP ($\times 10^{-9}$ g m/m^2 Pa.s)	CA (deg.)
Agar	1.90 ± 0.14^a	41.6 ± 0.8^b
Agar/CNC1 (5%)	2.15 ± 0.13^b	35.9 ± 1.2^c
Agar/CNC2 (5%)	2.13 ± 0.24^b	39.9 ± 1.2^b
Agar/CNC3 (5%)	1.95 ± 0.05^a	39.1 ± 1.2^b
Agar/CNC3 (1%)	1.85 ± 0.03^a	40.4 ± 1.6^b
Agar/CNC3 (3%)	1.91 ± 0.10^a	39.2 ± 1.5^b
Agar/CNC3 (5%)	1.95 ± 0.05^a	39.1 ± 1.2^b
Agar/CNC3 (10%)	2.44 ± 0.11^b	46.2 ± 1.5^a

[a] Each value is the mean of three replicates with the standard deviation. Any two means in the same column followed by the same letter are not significantly ($p > 0.05$) different by Duncan's multiple range test.

presumably due to that neutralization with NaOH for the preparation of CNC3 might induce enhanced reactivity of the CNC (Buschle-Diller & Zeronian, 1992) and increased dispersion of nanocrystals (as evidenced by the SEM results) increased interaction between the CNC and agar polymer matrix. The elongation at break (E) of agar film was not influenced by blending with 5 wt% of CNCs though it slightly increased when CNC3 was used. This tensile test result indicated that the CNC3 was more effective than the other types of CNCs to improve the mechanical properties of the composite film.

The effect of different concentration of CNC3 (0, 1, 3, 5, and 10%) on the mechanical properties of agar film is also shown in Table 2. The tensile strength (TS) of agar film increased with increase in CNC3 concentration up to 5 wt%, and decreased significantly ($p < 0.05$) when 10 wt% of CNC3 was incorporated. The decrease in TS of the composite film prepared with 10 wt% of CNC3 may be attributed to the formation of agglomeration of CNC and consequent decrease in interaction between CNC and agar polymer matrix, which was evidenced by the SEM analysis (Savadekar et al., 2014). The effect of CNC3 concentration on the EM of the composite films was similar to that of the *TS*. On the contrary, the flexibility (*E*) of the composite film increased by blending with 1 wt% of CNC3, then decreased slightly with increase in CNC3 concentration and decreased profoundly when added 10 wt% of CNCs. Similar effect of cellulose on tensile properties have been reported with agar/mulberry pulp nanocellulose (Reddy & Rhim, 2014), plasticized starch/cotton linter cellulose crystals (Lu et al., 2005), soy protein isolate/cellulose whiskers composite films (Wang, Cao, & Zhang, 2006), and cellulose nanocrystal reinforced polyethylene oxide films (Xu et al., 2014).

3.8. Water vapor permeability (WVP) and contact angle (CA) of films

The water vapor permeability (WVP) and water contact angle (CA) of agar and agar/CNCs composite films are shown in Table 3. The WVP of agar film was 1.90×10^{-9} g.m/m^2.Pa.s, but that of agar/CNC composite films changed depending on the type of CNCs used. Namely, it increased significantly ($p < 0.05$) when the agar film was blended with 5 wt% of CNC1 or CNC2, however, it maintained the same level of WVP when blended with 5 wt% of CNC3. This result indicates that the CNC3 was more effective to improve the water vapor barrier property of the agar/CNC composite film compared with the other types of CNC. The results on the effect of different concentration of CNC3 (0, 1, 3, 5, and 10 wt%) on the WVP of agar/CNC3 composite films are also shown in Table 3. The WVP of the composite film blended with 1 wt% of CNC3 decreased slightly compared to that of the control agar film, though the difference is not significant ($p > 0.05$) statistically. It maintained the same level of WVP as the control agar film when blended with CNC3 up to 5 wt%, then it increased significantly ($p < 0.05$) at high concentration (10 wt%) of CNCs. The increased WVP of agar/CNC3 at high concentration of CNC3 is probably due to the agglomeration of the nanocrystals at high concentration of CNCs as observed by the SEM analysis. Similar results on the effect of CNC concentration on the WVP of agar/mulberry pulp nanocellulose composite film have been reported (Reddy & Rhim, 2014). They found that the WVP of the agar film decreased when it was composited with mulberry pulp nanocellulose at low concentration (less than 3 wt%), then it increased at higher concentration of the nanocellulose. The decreased WVP of the composite film at low concentration of CNC was explained by the increased tortuous pathway of water vapor diffusion caused by the well dispersion of impervious crystalline cellulose nanocrystals in the polymer matrix, on the contrary, the increased WVP at high concentration of CNC was due to agglomeration of the CNC in the polymer matrix (Reddy & Rhim, 2014).

Water contact angle (CA) is usually used as a measure of the surface wettability or hydrophilicity of biopolymer films. Results on the *CA* of agar and agar/CNCs composite films were also shown in Table 3. The CA of the control agar film was 41.6°, which indicates that the agar film is highly hydrophilic based on the criteria that biopolymer film with the CA less than 65° is considered as hydrophilic (Vogler, 1998). The hydrophilicity of the agar film is mainly attributed to hydrophilic hydroxyl and carboxyl groups of the biopolymer (Shankar et al., 2015). The CA of agar/CNC composite film was also affected by the type of CNCs. The CA of composite films blended with 5 wt% of CNC2 and CNC3 decreased slightly though it was not significant ($p > 0.05$), however, it decreased significantly ($p < 0.05$) when CNC1 was used. The decreased CA or increase in hydrophililcity of agar/CNC1 composite film was mainly attributed to the high content of polar sulfate groups in the CNC1 as shown in the EDS test results (Morais et al., 2013). The effect of concentration of CNC3 on the CA of agar/CNC3 composite films are also shown in Table 3. Except agar/CNC1(5%) and agar/CNC3(10%) composite films, the CA of the composite films did not change significantly ($p > 0.05$) compared with the control agar film. However, it increased significantly ($p < 0.05$) when CNC3 concentration increased to 10 wt%. The increased CA of the agar/CNC3 composite film with high concentration of the CNC (10%) was presumably due to the rough surface of the film which was attributed to the CNC agglomeration as evidenced by the SEM observation.

4. Conclusions

Cellulose nanocrystals (CNCs) was isolated from cotton linter pulp fiber using different post purification methods after acid hydrolysis of the fiber, which include CNC1 (without post purification), CNC2 (dialyzed against distilled water), and CNC3 (neutralized with NaOH), and their reinforcing effect was evaluated by preparation of agar/CNCs composite films. Among the three different types of CNCs, the CNC3 showed higher thermal stability with comparable crystallinity than the other types of CNCs. In addition, the film performance properties, such as optical, mechanical, and water vapor barrier properties, of CNC3 incorporated agar-based composite film were superior to those prepared with other types of CNCs. The film properties of agar/CNC3 composite films also depended on the concentration of CNC3 added. All the performance properties of the composite film exhibited the maximum properties at the concentration of 5 wt% of CNC3 incorporation, then decreased at high concentration of CNC3. The present results suggested that the CNC3 can be used for the preparation of biopolymer-based composite films with improved properties instead of CNC2 prepared with time-consuming procedure. The CNC preparation method proposed in the present study, a simple neutralization acid hydrolyzed cellulose nanocrystals by NaOH is a simple, economic, and efficient way to use the CNC, and

it has a high potential to be used for the large scale production of crystalline cellulose nanocrystals for the utilization as a nanofiller for the preparation of biopolymer-based composite films.

Acknowledgement

This research was supported by the Agriculture Research Center (ARC 710003) program of the Ministry for Agriculture, Food and Rural Affairs, Korea.

References

Alemdar, A., & Sain, M. (2008). Isolation and characterization of nanofibrils from agricultural residues-wheat straw and soy hulls. *Bioresource Technology*, *99*, 1664–1671.
Azizi Samir, M. A. S., Alloin, F., & Dufresne, A. (2005). Review of recent research into cellulosic whiskers, their properties and their application in nanocomposite field. *Biomacromolecules*, *6*, 612–626.
Beck-Candanedo, S., Roman, M., & Gray, D. G. (2005). Effect of reaction conditions on the properties and behavior of wood cellulose nanocrystal suspensions. *Biomacromolecules*, *6*, 1048–1054.
Bledzki, A. K., & Gassan, J. (1999). Composites reinforced with cellulose-based fibers. *Progress in Polymer Science*, *24*, 221–274.
Buschle-Diller, G., & Zeronian, S. H. (1992). Enhancing the reactivity and strength of cotton fibers. *Applied Polymer Science*, *45*, 967–979.
Chang, C.-P., Wang, I.-C., Hung, K.-J., & Perng, Y.-S. (2010). Preparation and characterization of nanocrystalline cellulose by acid hydrolysis of cotton linter. *Taiwan Journal for Science*, *25*, 251–264.
Chen, W. S., Yu, H. P., Liu, Y. X., Chen, P., Zhang, M. X., & Hai, Y. F. (2011). Individualization of cellulose nanofibers from wood using high-intensity ultrasonication combined with chemical pretreatments. *Carbohydrate Polymers*, *83*, 1804–1811.
Chinga-Carrasco, G., & Syverud, K. (2010). Computer-assisted quantification of the multi-scale structure of films made of nanofibrillated cellulose. *Journal of Nanoparticle Research*, *12*, 841–851.
Gennadios, A., Weller, C. L., & Gooding, C. H. (1994). Measurement errors in water vapor permeability of highly permeable, hydrophilic edible films. *Journal of Food Engineering*, *21*, 395–409.
Gimenez, B., Lopez de Lacey, A., Perez-Santín, E., Lopez-Caballero, M. E., & Montero, P. (2013). Release of active compounds from agar and agar-gelatin films with green tea extract. *Food Hydrocolloids*, *30*, 264–271.
Gumuskaya, E., Usta, M., & Kirci, H. (2003). The effects of various pulping conditions on crystalline structure of cellulose in cotton linters. *Polymer Degradation and Stability*, *81*, 559–564.
Henriksson, M., Henriksson, G., Berglund, L. A., & Lindstrorn, T. (2007). An environmentally friendly method for enzyme-assisted preparation of microfibrillated cellulose (MFC) nanofibers. *European Polymer Journal*, *43*, 3434–3441.
Jiang, F., & Hsieh, Y.-L. (2013). Chemically and mechanically isolated nanocellulose and their self-assembled structures. *Carbohydrate Polymers*, *95*, 32–40.
Kanmani, P., & Rhim, J. W. (2014). Antimicrobial and physical-mechanical properties of agar-based films incorporated with grapefruit seed extract. *Carbohydrate Polymers*, *102*, 708–716.
Kontturi, E., Tammelin, T., & Osterberg, M. (2006). Cellulose-model films and the fundamental approach. *Chemical Society Reviews*, *35*, 1287–1304.
Li, Q., Zhou, J., & Zhang, L. (2009). Structure and properties of the nanocomposite films of chitosan reinforced with cellulose whiskers. *Journal of the Polymer Science Part B: Polymer Physics*, *47*, 1069–1077.
Li, J., Wei, X., Wang, Q., Chen, J., Chang, G., Kong, L., Su, J., & Liu, Y. (2012). Homogeneous isolation of nanocellulose from sugarcane bagasse by high pressure homogenization. *Carbohydrate Polymers*, *90*, 1609–1613.
Li, Y., Zhu, H., Xu, M., Zhuang, Z., Xu, M., & Dai, H. (2014). High yield preparation method of thermally stable cellulose nanofibrils. *BioResources*, *9*, 1986–1997.
Lu, P., & Hsieh, Y. L. (2012). Preparation and characterization of cellulose nanocrystals from rice straw. *Carbohydrate Polymers*, *87*, 564–573.
Lu, P., & Hsieh, Y.-L. (2010). Preparation and properties of cellulose nanocrystals: Rods, spheres, and network. *Carbohydrate Polymers*, *82*, 329–336.
Lu, Y., Weng, L., & Cao, X. (2005). Biocomposites of plasticized starch reinforced with cellulose crystallites from cottonseed linter. *Macromolecular Bioscience*, *5*, 1101–1107.
Maiti, S., Jayaramudu, J., Das, K., Reddy, S. M., Sadiku, R., Ray, S. S., et al. (2013). Preparation and characterization of nano-cellulose with new shape from different precursor. *Carbohydrate Polymers*, *98*, 562–567.
Morais, J. P. S., Rosa, M. F., Filho, M. M. S., Nascimento, L. D., Nascimento, D. M., & Cassales, A. R. (2013). Extraction and characterization of nanocellulose structures from raw cotton linter. *Carbohydrate Polymers*, *91*, 229–235.
Nazir, M. S., Wahjoedi, B. A., Yussof, A. W., & Abdullah, M. A. (2013). Eco-friendly extraction and characterization of cellulose from oil palm empty fruit bunches. *BioResources*, *8*, 2161–2172.
Reddy, J. P., & Rhim, J. W. (2014). Characterization of bionanocomposite films prepared with agar and paper-mulberry pulp nanocellulose. *Carbohydrate Polymers*, *110*, 480–488.
Reddy, K. O., Maheswari, C. U., Reddy, D. J. P., Guduri, B. R., & Rajulu, A. V. (2010). Properties of ligno-cellulose *Ficus religiosa* leaf fiber. *International Journal of Polymers and Technologies*, *2*, 29–35.
Rhim, J. W., Park, H.-M., & Ha, C.-S. (2013). Bio-nanocomposites for food packaging applications. *Progress in Polymer Science*, *38*, 1629–1652.
Rhim, J. W. (2011). Effect of clay contents on mechanical and water vapor barrier properties of agar-based nanocomposite films. *Carbohydrate Polymers*, *86*, 691–699.
Rhim, J. W., & Wang, L. F. (2013). Mechanical and water barrier properties of agar/K-carrageenan/konjac glucomannan ternary blend biohydrogel films. *Carbohydrate Polymers*, *96*, 71–81.
Rhim, J. W., Reddy, J. P., & Luo, X. (2015). Isolation of cellulose nanocrystals from onion skin and their utilization for the preparation of agar-based bio-nanocomposites films. *Cellulose*, *22*, 407–420.
Rhim, J. W., Wang, L.-F., Lee, Y., & Hong, S.-I. (2014). Preparation and characterization of bio-nanocomposite films of agar and silver nanoparticles: Laser ablation method. *Carbohydrate Polymers*, *103*, 456–465.
Roman, M., & Winter, W. T. (2004). Effect of sulfate groups from sulfuric acid hydrolysis on the thermal degradation behavior of bacterial cellulose. *Biomacromolecules*, *5*, 1671–1677.
Rosa, M. F., Medeiros, E. S., Malmonge, J. A., Gregorski, K. S., Wood, D. F., Mattoso, L. H. C., Glenn, G., Orts, W. J., & Imam, S. H. (2010). Cellulose nanowhiskers from coconut husk fibers: Effect of preparation conditions on their thermal and morphological behavior. *Carbohydrate Polymers*, *81*, 83–92.
Santos, T. M., Filho, M. S. M. S., Caceres, C. A., Rosa, M. F., Morais, J. P. S., Pinto, A. M. B., & Azeredo, H. M. C. (2014). Fish gelatin films as affected by cellulose whiskers and sonication. *Food Hydrocolloids*, *41*, 113–118.
Savadekar, N. R., Karande, V. S., Vigneshwaran, N., Kadam, P. G., & Mhaske, S. T. (2014). Preparation of cotton linter nanowhiskers by high-pressure homogenization process and its application in thermoplastic starch. *Applied Nanoscience*, http://dx.doi.org/10.1007/s13204-014-0316-3
Shankar, S., Reddy, J. P., Rhim, J. W., & Kim, H. Y. (2015). Preparation, characterization, and antimicrobial activity of chitin nanofibrils reinforced carrageenan nanocomposite films. *Carbohydrate Polymers*, *117*, 468–475.
Shankar, S., Teng, X., & Rhim, J.-W. (2014). Properties and characterization of agar/CuNP bionanocomposite films prepared with different copper salts and reducing agents. *Carbohydrate Polymers*, *114*, 484–492.
Teixeira, E. D., Correa, A. C., Manzoli, A., Leite, F. D., Oliveira, C. R., & Mattoso, L. H. C. (2010). Cellulose nanofibrils from white and naturally colored cotton fibers. *Cellulose*, *17*, 595–606.
Vogler, E. A. (1998). Structure and reactivity of water at biomaterial surfaces. *Advances in Colloid and Interface Science*, *74*, 69–117.
Wada, M., Heux, L., & Sugiyama, J. (2004). Polymorphism of cellulose I family: Reinvestigation of cellulose IVI. *Biomacromolecules*, *5*, 1385–1391.
Wada, M., Kondo, T., & Okano, T. (2003). Thermally induced crystal transformation from cellulose Iα to Iβ. *Polymer Journal*, *35*.
Wang, N., Ding, E., & Cheng, R. (2007). Thermal degradation behaviors of spherical cellulose nanocrystals with sulfate groups. *Journal of Polymer*, *48*, 3486–3493.
Wang, Y., Cao, X., & Zhang, L. (2006). Effects of cellulose whiskers on properties of soy protein thermoplastics. *Macromolecular Bioscience*, *6*, 524–531.
Xu, X., Liu, F., Jiang, L., Zhu, J. Y., Haagenson, D., & Wiesenborn, D. P. (2013). Cellulose nanocrystals vs. cellulose nanofibrils: A comparative study on their microstructures and effects as polymer reinforcing agents. *Applied Materials & Interfaces*, *5*, 2999–3009.
Xu, X., Wang, H., Jiang, L., Wang, X., Payne, S. A., Zhu, J. Y., & Li, R. (2014). Comparison between cellulose nanocrystal and cellulose nanofibril reinforced poly (ethylene oxide) nanofibers and their novel shish kebab-like crystalline structures. *Macromolecules*, *47*, 3409–3416.